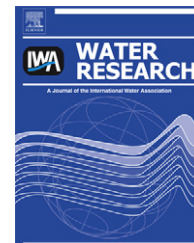


Available at www.sciencedirect.comjournal homepage: www.elsevier.com/locate/watres

A two-class population balance equation yielding bimodal flocculation of marine or estuarine sediments

Byung Joon Lee^{a,*}, Erik Toorman^a, Fred J. Molz^b, Jian Wang^a

^aHydraulics Laboratory, Department of Civil Engineering, Katholieke University of Leuven, Kasteelpark Arenberg 40, B-3001 Heverlee, Belgium

^bDepartment of Environmental Engineering & Earth Sciences, Clemson University, 342 Computer Court, Anderson, SC 29625, USA

ARTICLE INFO

Article history:

Received 16 June 2010

Received in revised form

23 December 2010

Accepted 23 December 2010

Available online 31 December 2010

Keywords:

Sediment

Flocculation

Population balance equation

Bimodal

Microfloc

Macrofloc

ABSTRACT

Bimodal flocculation of marine and estuarine sediments describes the aggregation and breakage process in which dense microflocs and floppy macroflocs change their relative mass fraction and develop a bimodal floc size distribution. To simulate bimodal flocculation of such sediments, a Two-Class Population Balance Equation (TCPBE), which includes both size-fixed microflocs and size-varying macroflocs, was developed. The new TCPBE was tested by a model-data fitting analysis with experimental data from 1-D column tests, in comparison with the simple Single-Class PBE (SCPBE) and the elaborate Multi-Class PBE (MCPBE). Results showed that the TCPBE was the simplest model that is capable of simulating the major aspects of the bimodal flocculation of marine and estuarine sediments. Therefore, the TCPBE can be implemented in a large-scale multi-dimensional flocculation model with least computational cost and used as a prototypic model for researchers to investigate complicated cohesive sediment transport in marine and estuarine environments. Incorporating additional biological and physicochemical aspects into the TCPBE flocculation process is straight-forward also.

© 2011 Elsevier Ltd. All rights reserved.

1. Introduction

Bimodal flocculation describes the aggregation and breakage process in which dense microflocs and floppy macroflocs change their relative mass fraction and develop a bimodal floc size distribution (FSD) with two peaks in the mass or volumetric size distribution of sediment flocs (Manning et al., 2007a; Mietta et al., in press; Verney et al., 2009; van Leussen, 1994). Bimodal flocculation has often been observed in marine and estuarine environments, especially in turbidity maximum zones which involve dynamic fronts between fresh and brackish water (Burd and Jackson, 2002; Chen et al., 2005; Curran et al., 2002, 2004, 2007; Hill et al., 2000; Jackson, 1995; Jackson et al., 1995; Li et al., 1993, 1999; Manning et al., 2006, 2007a, b; Manning and Bass, 2006; Mietta et al., in press;

Mikkelsen et al., 2006; Mikkelsen and Pejrup, 2001; van Leussen, 1994; Yuan et al., 2009). For example, a mixing process between microflocs supplied from an upstream river and macroflocs matured in an estuary was proposed as a cause of an observed bimodal FSD (Orange et al., 2005). Also, floc erosion and re-suspension from the bottom layer can enhance a bimodal FSD (Yuan et al., 2009). In this paper, however, we are interested mainly in internal causes of bimodal flocculation, rather than that due to simple mixing of different size classes of flocs.

Internally, bimodal flocculation can occur due to primary and secondary particle/floc binding mechanisms. The primary binding mechanism is characterized by direct contact between clay particles (e.g. the face-to-face or face-to-edge bonding between clay particles), whereas the secondary

* Corresponding author. Tel.: +32 16 321672; fax: +32 16 321989.

E-mail address: joon.lee@bwk.kuleuven.be (B.J. Lee).

0043-1354/\$ – see front matter © 2011 Elsevier Ltd. All rights reserved.

doi:10.1016/j.watres.2010.12.028

binding mechanism is by loose agglomeration between microflocs including the effects of heterogeneous inorganic or organic materials (e.g. polymeric bridging between microflocs) (van Leussen, 1994; Winterwerp and van Kesteren, 2004). The primary binding mechanism is strong but size-limited, whereas the secondary is weak but size-extending. Thus, the primary and secondary binding mechanisms play the distinct roles of packing less-porous and hard microflocs and agglomerating highly-porous and floppy macroflocs, respectively. As long as the flocculation process of a cohesive sediment is governed by both the primary and secondary binding mechanisms in a fluid shear field, the cohesive sediment will soon develop a bimodal FSD due to a mixture of resistant microflocs and fragile macroflocs. When the effects of a typical tidal cycle are included, the relative mass fractions of microflocs and macroflocs will continuously change while maintaining a bimodal FSD (Manning et al., 2006, 2007b; Manning and Bass, 2006; Winterwerp, 2002).

Marine and estuarine sediments are composed of heterogeneous particles with varying size, shape, mineralogy and so on. Such variability has been reported to enhance bimodal flocculation. For example, clay and silt have different particle binding capabilities and thus may be involved in bimodal flocculation. Considering that silt has the smaller contact area and higher density for a unit volume than clay flocs, it must have a lower binding capability, and thus may fail to build macroflocs above a certain size range (Li et al., 1993, 1999; Manning et al., 2007a). Similarly, heterogeneous mineral content can also limit floc size. For instance, smectite was found to remain in fragmented microflocs rather than in aggregated macroflocs because it has a smaller particle binding capability than other minerals (Li et al., 1999).

Natural organic matter can also enhance bimodal flocculation by modifying the primary and secondary binding mechanisms. The “gluing capacity” of such materials can enhance the building of macroflocs from constituent microflocs. Among various natural organic matter, linear polymeric organic materials, such as polysaccharides produced by benthic organisms, are known for enhancing inter-particle polymeric bridges (Chen et al., 2005; Manning et al., 2006, 2007a,b; Manning and Bass, 2006; Mietta et al., in press; Mikkelsen et al., 2006; van Leussen, 1994; Verney et al., 2009). The resulting macroflocs composed of polymeric organic matter and inorganic microflocs have large and floppy structures, and are often called “marine snow” to differentiate them from more compact flocs (Droppo et al., 2005). Floc sizes of marine and estuarine sediments were found to span from hundreds to thousands of micrometers in the organic-enriched condition, but only from tens to a few hundred micrometers in the organic-free condition (Chen et al., 2005; Manning et al., 2006, 2007a,b; Manning and Bass, 2006; Mietta et al., 2009, in press; Mikkelsen et al., 2006; van Leussen, 1994; Verney et al., 2009). Clearly, bimodal flocculation mechanisms are common and important to understand (Chen et al., 2005; Manning et al., 2006, 2007b; Manning and Bass, 2006; Mikkelsen et al., 2006).

Irrespective of the common occurrence of bimodal flocculation in estuarine and marine environments, most of the contemporary flocculation models simply assume that flocs have a single spatial-averaged size, with an underlying

unimodal FSD. Such output may result from a single-class population balance equation (SCPBE) or a concentration-dependent empirical equation (settling velocity versus solid concentration) (van Rijn, 1984, 2007; van Leussen, 1994; Winterwerp, 2002; Winterwerp and van Kesteren, 2004; Perianez, 2005; Son and Hsu, 2008, 2009; Maggi, 2009). However, it is obvious that single size class flocculation models have a fundamental limitation in approximating a bimodal FSD. For example, a single-class flocculation model cannot estimate the collecting capability of matured macroflocs in a marine or estuarine system for fresh microflocs supplied from an upstream river (Winterwerp, 2002; Winterwerp and van Kesteren, 2004). From both engineering and ecological viewpoints, the particle collecting capability of a marine or estuarine system is very important for such activities as determining a dredging schedule for a navigation channel or evaluating the environmental and ecological impact of siltation. Effort to overcome the limitation of the contemporary single-class flocculation models recently started by developing a size class-based model and a distribution-based model, which can simulate a floc distribution of distinct size classes and an underlying continuous distribution of an average radius, respectively (Verney et al., in press; Maerz et al., in press).

Beside those state-of-the-art flocculation models, a simplified two-class population balance equation (TCPBE) was developed and tested to overcome the drawbacks of the single size class flocculation models while maintaining simplicity. This TCPBE consists of two particle classes, a size-fixed microfloc and size-varying macrofloc, a minimum requirement to approximate bimodal flocculation. The size-fixed microflocs decrease in number concentration as they combine with macroflocs, but by definition they do not change size with time. The macroflocs change size with time, but again by definition the TCPBE yields only the average macrofloc size as a function of time. The two resulting floc sizes at a given time are used to approximate the two modal or average values of a true bimodal FSD. Based on a generic equation used in the crystallization process, the TCPBE was further modified for marine and estuarine sediments by discarding the nucleation process (forming solid nuclei with dissolved molecules) while maintaining the shear-induced breakage process (Jeong and Choi, 2003, 2004, 2005; Megaridis and Dobbins, 1990; Mueller et al., 2009a,b). The validity and applicability of the new TCPBE was tested with experimental data obtained from 1-D settling column tests (van Leussen, 1994), and compared with results from the simple SCPBE and the more elaborate multi-class PBE (MCPBE), which, at considerable computational expense, allows both floc size and number density to change with space and time so that an actual time-dependent bimodal floc size distribution results.

2. Model description and numerical methods

One of the most realistic ways to simulate flocculation and non-homogeneous turbulent settling in a multi-dimensional space is by applying Population Balance Equations (PBE) within a Computational Fluid Dynamics (CFD) framework

(Krishnappan and Marsalek, 2002; Fox, 2003; Prat and Ducoste, 2006). Following Prat and Ducoste (2006), a generic and general mathematical model for the PBEs in a multi-dimensional fluid field may be written as:

$$\left[\frac{\partial n_i}{\partial t} \right] \tag{I}$$

$$+ \left[\frac{\partial}{\partial x}(u_x n_i) + \frac{\partial}{\partial y}(u_y n_i) + \frac{\partial}{\partial z}(u_z n_i) \right] \tag{II}$$

$$- \left[\frac{\partial}{\partial x} \left(D_{tx} \frac{\partial n_i}{\partial x} \right) + \frac{\partial}{\partial y} \left(D_{ty} \frac{\partial n_i}{\partial y} \right) + \frac{\partial}{\partial z} \left(D_{tz} \frac{\partial n_i}{\partial z} \right) \right] \tag{III}$$

$$= (A_i + B_i) - \frac{\partial(w_{s,i} n_i)}{\partial z} \tag{IV}$$

In Equation (1), $n_i = n(x,y,z,D_i,t)$ = number concentration of the i th particle size class with a particle diameter of D_i ($i = 1, 2, \dots, i_{max}$; $D_1 \leq D_i \leq D_{max}$; for all D , n is called the population density function), x, y, z, t = position and time, u_x, u_y, u_z = mean fluid velocities in the x, y and z directions, D_{tx}, D_{ty}, D_{tz} = turbulent dispersion coefficients in the x, y and z directions, A_i and B_i = growth and decay kinetics of n_i by aggregation and breakage, respectively, and $w_{s,i}$ = settling velocity of the i th particle class due to gravity. On the left-hand side of Equation (1), the respective terms in brackets represent the storage change (I), the particle mean advection (II), and the turbulent diffusion of flocs (III), while on the right-hand side, the source/sink terms (IV) represent the net effects of floc aggregation, breakage and settling due to gravity. The quantities depending on fluid variables (u and D_i) couple Equations (1) to the turbulent fluid dynamics equations. The aggregation and breakage kinetics, to be discussed later, form the core of the multi-dimensional PBEs because they largely determine floc size and settling velocity. In a 0-dimensional case, the aggregation and breakage kinetics ($A_i + B_i$) can stand alone without the other space-dependent terms. The problem with the general form of this model is that the number (i) of discrete floc sizes can be huge, numbering in the thousands or millions. This problem is usually simplified by defining groups or classes of flocs that contain a range of discrete floc sizes.

2.1. A multi-class population balance equation

Following the multi-class discretization scheme proposed by Hounslow et al. (1988) and Spicer and Pratsinis (1996), a set of floc size classes are defined such that each class contains all discrete flocs up to a maximum floc size that is two times the maximum floc size contained in the previous smaller class. Thus if δ -sized floc monomers were linearly organized in this way, class 1 would contain flocs of size “ δ ”, class 2 would contain flocs of size “ 2δ ”, class 3 would contain sizes “ 3δ ” and “ 4δ ”, class 4 would contain “ 5δ ” through “ 8δ ”, class 5 would contain “ 9δ ” through “ 16δ ”, and so on. Since the maximum floc size in class “ i ” increases as $2^{(i-1)}$, 30 mean classes will contain floc sizes varying from “ δ ” to “ $2^{29}\delta$ ”, which represents a growth factor of more than 537 million. However, the MCPBE still requires about 30 floc size classes and differential equations for spherical and porous flocs to cover from several micrometers to millimeters (according to the floc packing strategy of the fractal theory, $D_i = \delta \cdot (2^{i-1})^{1/n_f}$; $1 < n_f < 3$ for spherical and porous flocs) (Spicer and Pratsinis, 1996). Thus, the MCPBE will still have computational difficulties in higher dimensional problems. Also, much expensive experimental study is

required in order to quantify the many parameters involved and realize the full capability of the MCPBE formulation.

The differential equations of the 1-dimensional version of the MCPBE without fluid advection are formulated as Equation (2) and tested with experimental data from a 1-dimensional settling column test (van Leussen, 1994):

$$\frac{dn_i}{dt} - \frac{\partial}{\partial z} \left(D_{tz} \frac{\partial n_i}{\partial z} \right) = (A_i + B_i) - \frac{\partial(w_{s,i} n_i)}{\partial z}$$

$$A_i = n_{i-1} \sum_{j=1}^{i-2} 2^{j-i+1} \alpha \beta_{i-1-j} n_j + \frac{1}{2} \alpha \beta_{i-1,i-1} n_{i-1}^2 - n_i \sum_{j=1}^{i-1} 2^{j-i} \alpha \beta_{i,j} n_j$$

$$- n_i \sum_{j=i}^{(\max i)} \alpha \beta_{i,j} n_j$$

$$B_i = -a_i n_i + \sum_{j=i+1}^{(\max i)} b_{i,j} a_j n_j \tag{2}$$

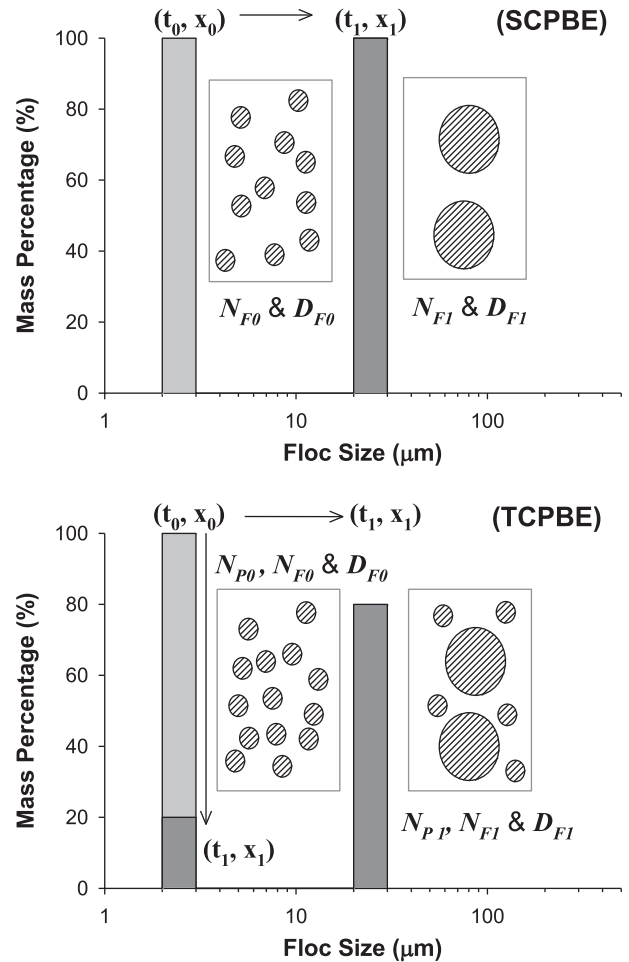

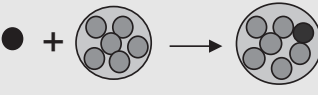
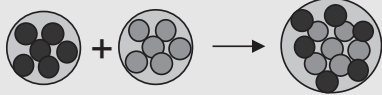
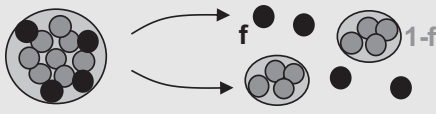


Fig. 1 – Flocculation strategies of the SCPBE and TCPBE, representing the time- and space-dependent change of the floc size distributions (FSDs). t and x represent time and spatial coordinate and change from 0 to 1 in a flocculation process. N_P and N_F are the number concentration of microflocs and macroflocs in suspension, respectively, D_F is the diameter of macroflocs, and N_C represents the number of microflocs bound in a macrofloc as a floc size index.

Table 1 – Aggregation and breakage processes of the TCPBE, shown in the Peterson matrix.

Process (j) ↓	Description	Component (i) →			Process rate ρ _j (/m ³ s ⁻¹)
		N _P	N _F	N _T (= N _F × N _C)	
(1) Collision Microflocs		$-\frac{1}{2}\left(\frac{N_C}{N_C-1}\right)$	$\frac{1}{2}\left(\frac{N_C}{N_C-1}\right)$	$\frac{1}{2}\left(\frac{N_C}{N_C-1}\right)$	$\alpha\beta_{PP}N_P N_P$
(2) Collision Micro & Macroflocs		-1		+1	$\alpha\beta_{PF}N_P N_F$
(3) Collision Macroflocs			$-\frac{1}{2}$		$\alpha\beta_{FF}N_F N_F$
(4) Breakage Macroflocs		+f·N _C	+1	-f·N _C	aN _F

Nomenclature: N_P = Number concentration of microflocs in suspension (/m³); N_F = Number concentration of macroflocs in suspension (/m³); N_T = Number concentration of microflocs in macroflocs (/m³); N_C = Number of microflocs in a macrofloc (-); α = Collision efficiency efficiency; β = Collision frequency frequency; a_F = Breakage kinetic function; f = Fraction of microflocs generated by breakage.

In Equation (2), A_i and B_i represent aggregation and breakage kinetics of n_i, respectively. Several empirical or theoretical factors or functions (α, β, a, and b) are incorporated into the aggregation and breakage kinetics. In the aggregation kinetics, the collision efficiency factor or the fraction of collisions that result in aggregation (0 ≤ α ≤ 1) describes the physicochemical properties of solid and liquid to cause inter-particle attachments, while the collision frequency factor or the rate at which particles of volumes V_i and V_j colloid (β) represents the mechanical fluid properties that induce inter-particle collisions. In experimental and modeling applications, the collision efficiency factor (α) is generally used as an application-specific fitting parameter and the collision frequency factor (β) is applied as a fixed theoretical function correlated with Brownian motion, shear rate, and differential settling. In the breakage kinetics, the breakage kinetic parameter (a) represents the speed of the breakage process and is generally applied as a shear- and size-dependent function. The breakage distribution function (b) represents the volume fraction of the fragments of size i coming from j-sized flocs. The binary breakage function, describing birth of two equally-sized daughter fragments from one parent floc, is given by Equation (3) (Kusters, 1991; Jackson, 1995; Spicer and Pratsinis, 1996; Ding et al., 2006).

$$\sum_{j=i+1}^{(\max i)} b_{ij} a_j n_j = b_{i,i+1} a_{i+1} n_{i+1} = 2a_{i+1} n_{i+1} \quad (3)$$

In this research, an additional breakage parameter (f) was incorporated in the binary breakage model to calculate the mass fraction of residual microflocs generated by breakage of

macroflocs. The modified binary breakage model is given by Equation (4).

$$\sum_{j=i+1}^{(\max i)} b_{ij} a_j n_j = \begin{cases} 2a_2 n_2 + \sum_{j=2}^{(\max i)} 2^{j-1} 2f a_{j+1} n_{j+1} & \text{for } i = 1 \\ 2(1-f) a_{i+1} n_{i+1} & \text{for } i = 2 \text{ to } \max i \end{cases} \quad (4)$$

Table 2 – Aggregation and breakage kinetic kernels and parameters of the SCPBE, MCPBE, and TCPBE.

PBE	Aggregation kernel	Breakage kernel	Kinetic constants
SCPBE	$\beta = \frac{1}{6}(2D_F)^3 G$	$a_i = E_b G \left(\frac{D_i - D_p}{D_p}\right)^p$	α, E _b
MCPBE	$\beta_{ij} = \beta_{BR,ij} + \beta_{SH,ij} + \beta_{DS,ij}$ $\beta_{BR,ij} = \frac{2kT}{3\mu} \left(\frac{1}{D_i} + \frac{1}{D_j}\right) (D_i + D_j)$	$\left(\frac{\mu G}{F_y/D_i^2}\right)^q$	α, E _b , f
TCPBE	$\beta_{SH,ij} = \frac{1}{6}(D_i + D_j)^3 G$ $\beta_{DS,ij} = \frac{3}{4}(D_i + D_j)^2 w_i - w_j $		α, E _b , f

Nomenclature: D_i = Diameter of a particle size class i (MCPBE); D_P, D_F = Diameter of a microfloc/macrofloc (SCPBE, TCPBE); D_F = N_C^{1/n_F} D_P (Fractal Theory); N_C = Number of microflocs bound in a macrofloc; n_F = Fractal Dimension; α = Collision efficiency factor; β_{i,j} = Collision frequency function between size classes i and j; β_{BR} = Collision frequency function by Brownian motion; β_{SH} = Collision frequency function by fluid shear; β_{DS} = Collision frequency function by discrete settling; k = Boltzmann's constant; p, q = Empirical parameters determined by experiments; T = Absolute Temperature (K); μ = Absolute viscosity of the fluid; G = (ε/ν)^{0.5} = Shear rate (/s); ε = Kinematic energy dissipation rate; ν = Kinematic viscosity; w_i = Sedimentation velocity of particle size class i; a_i = Breakage kinetic function (Maggi, 2005); E_b = Efficiency for the breakage process (Maggi, 2005); F_y = Yield strength of flocs (10⁻¹⁰ Pa) (Maggi, 2005); f = Fraction of microflocs generated by breakage.

Table 3 – Parameters and initial conditions used in the best-quality simulation.

Classification	Symbol	Value	Description
Kinetic parameters and physicochemical constants			
Agg/Brk Kinetics	α	0.20 0.30 0.10	Collision efficiency factor [-] (MCPBE SCPBE TCPBE)
	E_b	1.0e-4	Efficiency factor for breakage [$s^{0.5}/m$]
	F_y	1.0e-10	Yield strength of flocs [Pa]
	D_C	450	Critical diameter for floc growth [μm]
	f	0.10	Fraction of microflocs by breakage [-]
	p^a	1.0	Empirical parameter of breakage kinetics
	q	3.0 - n_f	Empirical parameter of breakage kinetics
Fluid Turbulence	σ	0.100	Frequency of the oscillating grid [/s]
	ϵ^b	5.36e-5	Kinematic energy dissipation rate [m^2/s^3]
	D_{tz}^b	1.07e-4	Vertical dispersion coefficient [$s^{0.5}/m$]
	G^b	7.31	Shear rate [/s]
Sediment Property	c	1.1	Mass conc. of the tested sediment [g/L]
	N_{PT}^c	2.25e+11	No. conc. of microflocs [$/m^3$]
	ρ_p	1600	Density of microflocs [kg/m^3]
	D_p	18.0	Diameter of microflocs [μm]
	n_f	2.0	Fractal dimension of macroflocs [-]
	a	4.0	Exponent of Richardson–Zaki eqn [Pa]
Initial Conditions (at $t = 0$)			
Seeded Macroflocs	$D_{F,0}$	50	Diameter of seeded macroflocs [μm]
	$Frac_{F,0}$	0.001	Mass fraction of seeded macroflocs [-]
MCPBE	$n_{1,0}$	$(1 - Frac_{F,0}) N_{PT}$	No. conc. of 1st size class [$/m^3$]
	$n_{4,0}$	$2^{-3} (Frac_{F,0}) N_{PT}$	No. conc. of seeded macroflocs [$/m^3$]
	$n_{i,0}$	0	No. conc. of other size classes [$/m^3$]
SCPBE	$N_{F,0}$	$1.0 N_{PT}$	No. conc. of primary flocs [$/m^3$]
TCPBE	$N_{p,0}$	$(1 - Frac_{F,0}) N_{PT}$	No. conc. of microflocs [$/m^3$]
	$N_{F,0}$	$(D_{F,0}/D_p)^{-inf (Frac_{F,0})} N_{PT}$	No. conc. of macroflocs [$/m^3$]
	$N_{T,0}$	$(Frac_{F,0}) N_{PT}$	Total no. conc. of microflocs [$/m^3$]

a p was set as 1.0 to narrow FSDs, instead of 0.5 of Winterwerp and van Kesteren (2004).

b $\epsilon = 127 a_0^3 \sigma^3$, $D_z = 0.19 a_0^2 \sigma$, and $G = \sqrt{\epsilon/\nu}$ (van Leussen, 1994), where, $a_0 = 0.075 =$ amplitude oscillating grid [m], $\nu = 1.10e-6 =$ kinematic viscosity [m^2/s].

c $N_{PT} = c/(0.167\pi D_p^3)/\rho_s$, assuming that a primary microfloc is spherical.

2.2. A single-class population balance equation

The 1-D form of the SCPBE selected for study is formulated as Equations (5) and (6), (Winterwerp, 2002; Winterwerp and van Kesteren, 2004; Son and Hsu, 2008, 2009). The single-class floc size (D_f) varies at different time and spatial points, because of transport and flocculation, but it is a single size value without any other floc size classes (Fig. 1). Thus, at a fixed time D_f may be viewed as the mean floc size of the floc size distribution that is actually present at each point. For the 1-dimensional simulation of a settling column test, the sediment transport equation ($\partial c/\partial t$) and the SCPBE ($\partial N_f/\partial t$) are solved in a coupled way, and the particle/floc diameter (D_f) is updated with Equation (6) (Winterwerp and van Kesteren, 2004). The SCPBE is easy to solve and results in a robust numerical simulation, but it cannot even approximate bimodal flocculation and differential settling-induced flocculation because it has a single floc size class at each point. Also, only fluid shear-induced flocculation is considered.

$$\frac{dN_f}{dt} - \frac{\partial}{\partial z} \left(D_{tz} \frac{\partial N_f}{\partial z} \right) = (A_f + B_f) - \frac{\partial (w_{s,f} N_f)}{\partial z} \quad (5)$$

$$(A_f + B_f) = -\frac{1}{2} \alpha \beta_{FF} N_f^2 + a N_f$$

$$D_f = \left(\frac{f \rho_s D_p^{3-n_f}}{c} N_f \right)^{-1/n_f} \quad (6)$$

In Equations (5) and (6), $N_f =$ number concentration of flocs, $\alpha =$ collision efficiency factor, $\beta =$ collision frequency factor, $a =$ breakage kinetic constant, $c =$ mass concentration of flocs, $D_f =$ floc size, $D_p =$ primary particle size, $f_s =$ shape factor (for spherical particles, $f_s = \pi/6$), $\rho_s =$ solid density.

2.3. A two-class population balance equation

In contrast to the single-class PBE, the selected two-class PBE is able to approximate bimodal flocculation i.e. the fate of residual microflocs and aggregating macroflocs, each in a single-class size sense. Therefore, the 1-D TCPBE, formulated as Equations (7), tracks the number concentration of microflocs and macroflocs and the size of macroflocs as the time- and space-dependent variables ($N_p(t,z)$, $N_f(t,z)$, and $D_f(t,z)$). This two-class PBE includes size-fixed microflocs and size-varying macroflocs, which describe primary building blocks and secondary agglomerates, respectively. The average size of macroflocs ($D_f(t,z)$) varies at different times and spatial points because of transport and flocculation, but no other macrofloc size classes are allowed. However, it is important to note that the size of the microflocs (D_p) in this model remain constant irrespective of time and space. The number of microflocs bound in a macrofloc (N_c) is used as a floc size index in the TCPBE. Because this new size index becomes one for microflocs ($N_c = 1$) and an integer for macroflocs ($N_c = i$),

instead of a real number of linear or volumetric size indices (D_P and D_F), it yields simplicity in mathematical formulation and computation to the TCPBE. As shown in Fig. 1, three variables – the number concentrations of microflocs and macroflocs in suspension (N_P and N_F) and the size index of macroflocs (N_C) – are unknown in time and space. Therefore, the TCPBE incorporates three coupled differential equations describing the time rate of change of: (1) the number concentration of microflocs in suspension (dN_P/dt), (2) the number concentration of macroflocs in suspension (dN_F/dt), and (3) the number concentration of microflocs bound in macroflocs (dN_T/dt) ($N_T = N_C \times N_F$) (Equation (7)). A more generic TCPBE was also derived by the moment conservation law of a floc size distribution (FSD) and explained in depth by Jeong and Choi (2003, 2004, 2005).

$$\begin{aligned} \frac{dN_P}{dt} - \frac{\partial}{\partial z} \left(D_{tz} \frac{\partial N_P}{\partial z} \right) &= (A_P + B_P) - \frac{\partial (w_{s,P} N_P)}{\partial z} \\ (A_P + B_P) &= -\frac{1}{2} \alpha \beta_{PP} N_P N_P \left(\frac{N_C}{N_C - 1} \right) - \alpha \beta_{PF} N_P N_F + f N_C a N_F \\ \frac{dN_F}{dt} - \frac{\partial}{\partial z} \left(D_{tz} \frac{\partial N_F}{\partial z} \right) &= (A_F + B_F) - \frac{\partial (w_{s,F} N_F)}{\partial z} \\ (A_F + B_F) &= +\frac{1}{2} \alpha \beta_{PP} N_P N_P \left(\frac{1}{N_C - 1} \right) - \frac{1}{2} \alpha \beta_{FF} N_F N_F + a N_F \\ \frac{dN_T}{dt} - \frac{\partial}{\partial z} \left(D_{tz} \frac{\partial N_T}{\partial z} \right) &= (A_T + B_T) - \frac{\partial (w_{s,T} N_T)}{\partial z} \\ (A_T + B_T) &= +\frac{1}{2} \alpha \beta_{PP} N_P N_P \left(\frac{N_C}{N_C - 1} \right) + \alpha \beta_{PF} N_P N_F - f N_C a N_F \end{aligned} \quad (7)$$

In Equation (7), the subscript P and F represent microfloc and macrofloc, respectively. f represents fraction of microflocs generated by breakage of macroflocs, whereas $1 - f$ is fraction of smaller macroflocs by breakage of larger macroflocs. α = collision efficiency factor, β = collision frequency factor, and a = breakage kinetic constant. The settling velocity of N_T ($w_{s,T}$) is equal to the settling velocity of N_F ($w_{s,F}$).

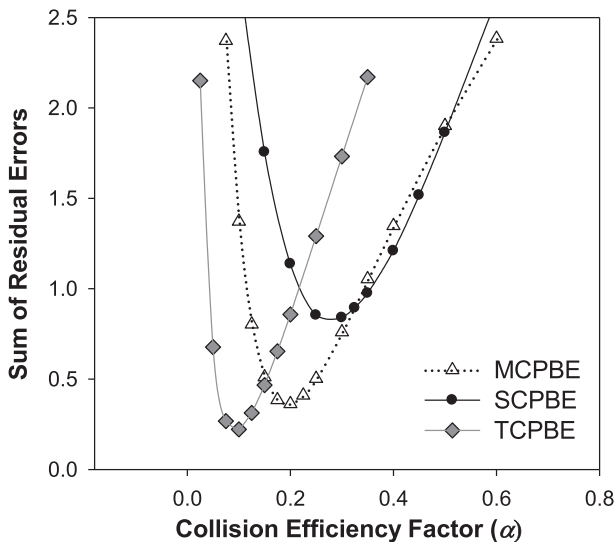


Fig. 2 – Plots of the sum of residual errors (SREs) versus collision efficiency factor (α) for the MCPBE (Triangles), SCPBE (Black Circles), and TCPBE (Gray Diamond). The SREs were calculated based on the difference between the measured and simulated concentration profiles while changing collision efficiency factor (α).

The aggregation and breakage kinetic equations of the TCPBE are shown in the Peterson matrix for better understanding (Table 1) (Peterson, 1965). Each aggregation and breakage kinetic equation of a component ($A_P + B_P$, $A_F + B_F$, or $A_T + B_T$) can be formulated by multiplying stoichiometric coefficients (ν_{ij}) with a process rate (ρ_i) and summing the multiplied terms ($A_i + B_i = \sum \nu_{ij} \rho_j$). The stoichiometric coefficients are shown in the third ~ fifth columns of Table 1 and the reaction rates are in the last column. The TCPBE includes four aggregation or breakage kinetic processes: (1) aggregation between microflocs, (2) aggregation between microflocs and macroflocs, (3) aggregation between macroflocs, and (4)

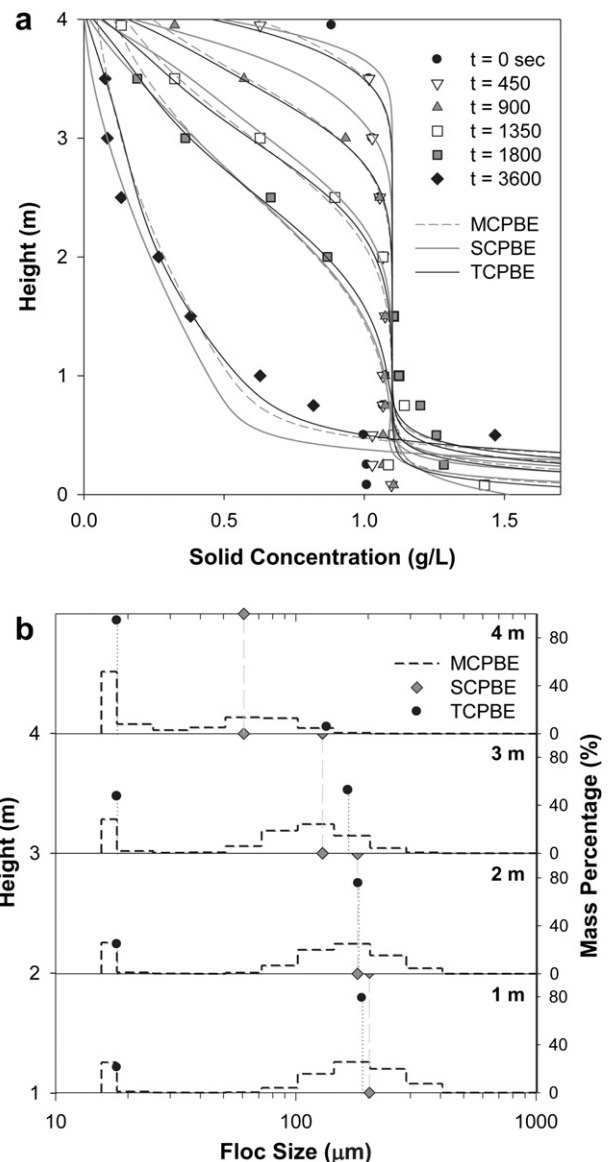


Fig. 3 – (a) Measured (symbols) and simulated solid concentration profiles of the best-quality simulations with the MCPBE, SCPBE, and TCPBE (lines) at time = 450, 900, 1350, 1800, and 3600 s. (b) The floc size distributions (FSDs) of the best-quality simulations with the MCPBE, SCPBE, and TCPBE. They were captured at a different water height of 1, 2, 3, or 4 m at $t = 1800$ s, and are plotted in the four separate figures.

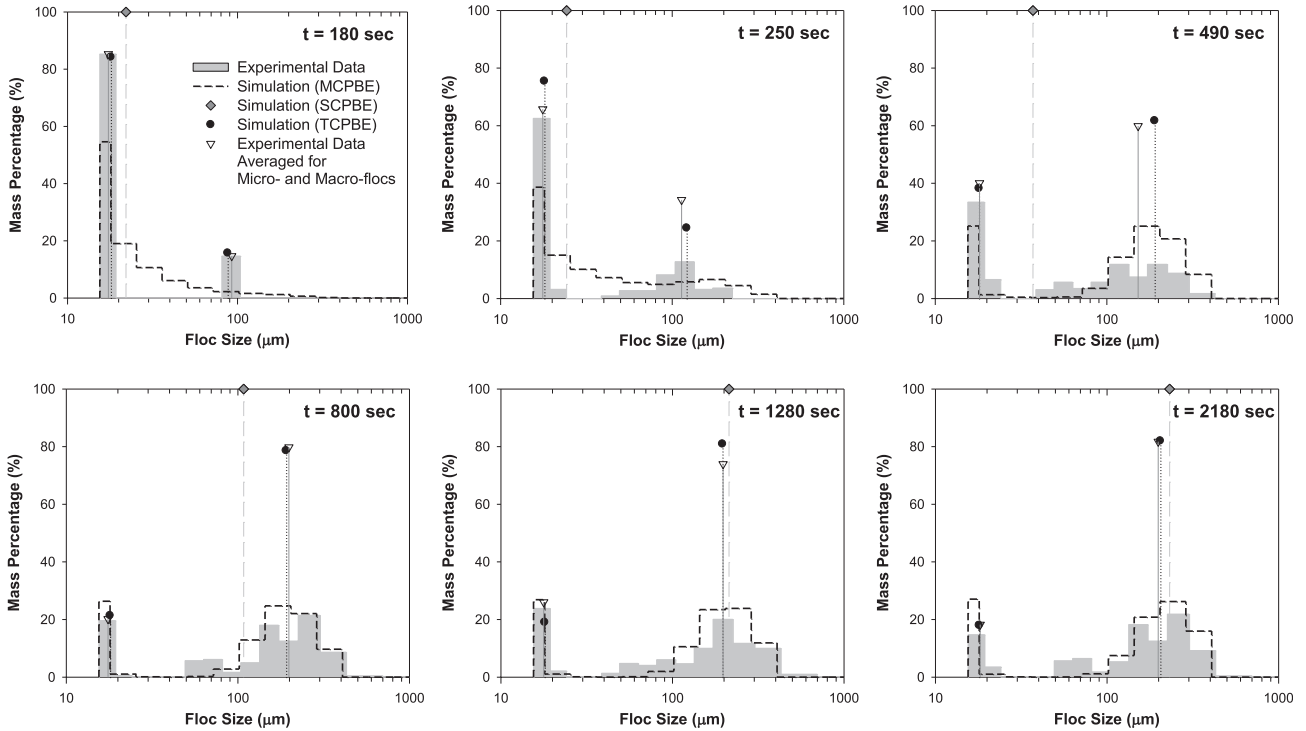


Fig. 4 – Measured floc size distributions (FSDs) (shaded area), the two peaks averaged from the measured FSD (triangle), and simulated FSDs of the best-quality simulations with the MCPBE (dashed line), SCPBE (diamond), and TCPBE (dark circle) at time = 180, 250, 490, 800, 1280, and 2180 s. FSDs were measured for settling flocs right above the concentrated bottom layer, to avoid the effect of floc deposition (van Leussen, 1994). Similarly, Simulated FSDs were obtained at 300 mm above the bottom of the settling column.

breakage of macroflocs. Again, an additional breakage parameter (f) was incorporated into the breakage process to calculate the mass fraction of microflocs generated by breakage of macroflocs. The TCPBE obtains higher computational efficiency than MCPBEs by omitting many floc size classes. In contrast to the SCPBE, the TCPBE is able to simulate interactions between microflocs and macroflocs. Thus, the TCPBE maintains much simplicity compared to the MCPBE but significantly more capability than the SCPBE.

2.4. Aggregation and breakage kernels and kinetic parameters

Table 2 summarizes the aggregation and breakage kernels and kinetic parameters of the MCPBE, SCPBE, and TCPBE. The aggregation and breakage kernels which are commonly used in marine and estuarine environments were adopted again in this research (van Leussen, 1994; Jackson, 1995; Winterwerp, 2002; Winterwerp and van Kesteren, 2004; Maggi, 2005). Noteworthy is that the MCPBE and TCPBE have the aggregation kernels by Brownian motion, differential settling, and fluid shear. However, the SCPBE has only the aggregation kernel by fluid shear (Winterwerp, 2002; Winterwerp and van Kesteren, 2004; Son and Hsu, 2008, 2009). For the breakage kernel, the shear-induced breakage kinetic function was adopted for all the PBEs (Winterwerp, 2002; Winterwerp and van Kesteren, 2004; Maggi, 2005). However, the contemporary PBEs and their kinetic kernels and parameters are not

capable of simulating flocculation in highly concentrated suspension in the hindered regime. In detail, the shear-induced breakage could not limit the infinite size growth of macroflocs in the highly concentrated bottom layer of an estuary or a settling column. Thus, an additional empirical parameter (D_c ; critical diameter) was introduced to prevent unrealistic floc size growth. Above the critical diameter (D_c), the breakage rate was set sufficiently high to break all flocs.

2.5. Floc settling equations

The modified Stokes equation, including the use of fractal theory for floc packing and shaping and Schiller’s equation for a particle drag effect, was used to calculate the floc settling velocity ($w_{s,i}$) (Schiller, 1932). The Richardson–Zaki equation was used to calculate the correction factor (Φ_{HS}) for hindered settling occurring in the highly concentrated bottom layer (Equations (8) and (9)) (Richardson and Zaki, 1954; Toorman, 1999; Winterwerp, 2002; Winterwerp and van Kesteren, 2004). The empirical parameters, the fractal dimension (n_f) and the exponent of the Richardson–Zaki equation (a), were reported to be 1.7–2.3 and 2.5–5.5, respectively, for estuarine and marine sediments, so they were fixed at 2.0 and 4.0 in this research (Winterwerp and van Kesteren, 2004).

$$w_{s,i} = \Phi_{HS} \left(\frac{1}{18} \frac{(\rho_s - \rho_w)g}{\mu} D_p^{3-n_f} \frac{D_i^{n_f-1}}{1 + 0.15Re_i^{0.687}} \right) \tag{8}$$

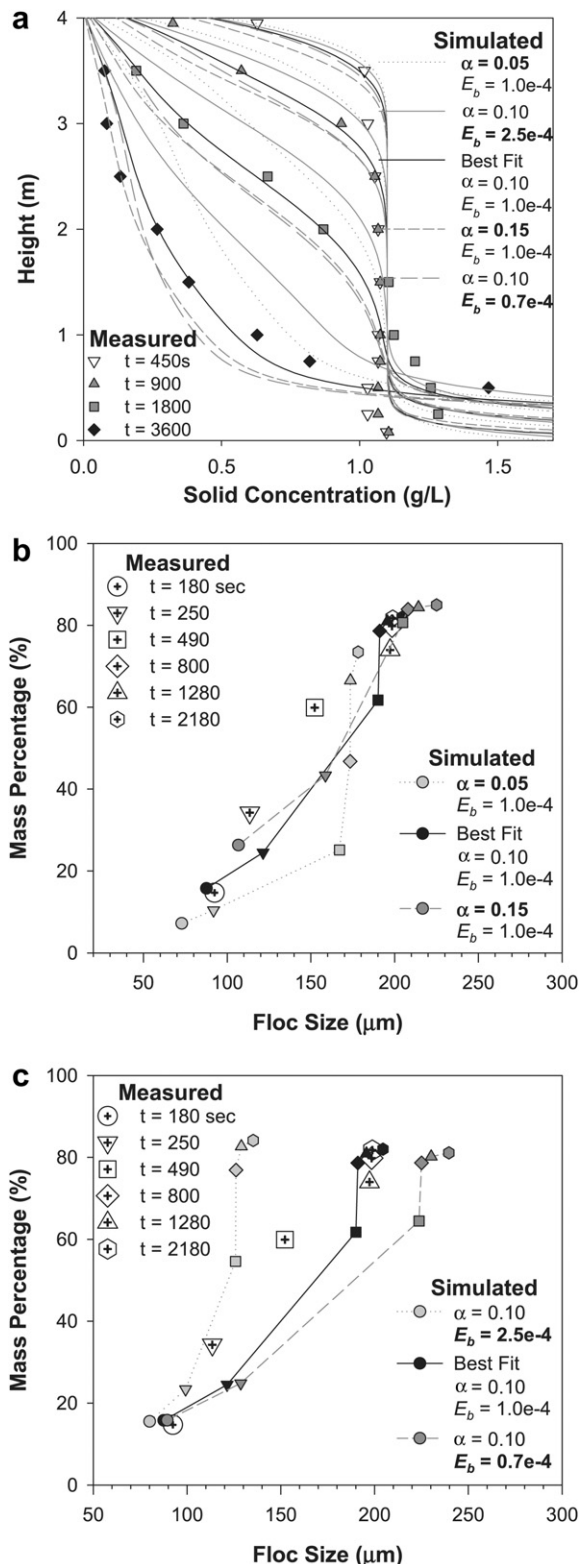


Fig. 5 – (a) Sensitivity of the solid concentration profiles of the TCPBE to the collision and breakage efficiency factors (α and E_b). Symbols represent measured solid concentration profiles at time = 450, 900, 1800, and 3600 s. Lines represent simulated profiles with different collision and breakage efficiency factors (α and E_b). (b) sensitivity of the size and mass fraction of macroflocs to the collision efficiency factor (α) and (c) sensitivity to the breakage

$$\Phi_{HS} = (1 - \phi)^a \quad (9)$$

In Equations (8) and (9), ρ_s = particle density, ρ_w = fluid density, g = gravitational acceleration, μ = fluid viscosity, Φ_{HS} = correction factor for hindered settling, Φ = volumetric concentration of flocs ($\text{m}^3 \text{Flocs}/\text{m}^3$) calculated by multiplying the volumetric size of a floc (m^3) and the number concentration of flocs ($1/\text{m}^3$), and Re_i = Reynolds number of a particle or floc.

2.6. Experimental and numerical methods

The 1-dimensional settling column test (van Leussen, 1994) provided both of the experimental indices, (1) solid concentration profiles and (2) FSDs (i.e. floc size and mass fraction), which were used for the comparative study between the PBEs and the sensitivity analyses of the TCPBE. The settling column had a 0.29 m diameter and a height of 4.25 m and was placed in a thermostatically controlled water bath. The homogeneous and isotropic intensity of a turbulence field was generated by means of axial oscillations of a grid installed inside the settling column (see van Leussen, 1994 for details). The intensity of a turbulence field was controlled by the alternating frequency of the oscillating grid (van Leussen, 1994; Maggi, 2005). To initiate the experiment, the settling column was filled with a mixture consisting of mud from the Ems estuary in the northern part of the Netherlands and salt water. This water/sediment mixture was adjusted to have a solids concentration of 1000 mg/L and a salinity of 32. The mixture was then homogenized at a very high oscillating speed of the inner grids ($\sigma = 4 \text{ Hz}$, $G = 1848/\text{s}$) until all the aggregates were destroyed down to the size of the initial microflocs. At the beginning of the test, the turbulent shear rate (G) was set at $7.31/\text{s}$ by adjusting the oscillating speed of the inner grids (σ) to 0.1 Hz (Table 3), and the experimental indices – solid concentration profiles and FSDs – were measured as a function of time. FSDs were measured with a Malvern 2600 particle sizer (Fraunhofer diffraction) for flocs collected near the bottom of the settling column. Detailed experimental methods and techniques of the 1-D settling column test may be found in van Leussen (1994).

The operator splitting algorithm and Gauss-Seidel iteration were applied to solve the nonlinear partial differential equations of the 1-dimensional PBEs (Equations (2), (5), (7)). According to the operator splitting algorithm, the transport (advection–diffusion) and source/sink (reaction–settling) operators were decoupled and sequentially solved in each time step, to cope with the complexity and nonlinearity of the PBEs (Aro et al., 1999; Winterwerp, 2002; Winterwerp and van Kesteren, 2004). This decoupling strategy separating the complex reaction–settling operator may be useful for solving a large-scale multi-dimensional flocculation system. Each operator was solved using Gauss-Seidel iteration, in which the dependent variables are updated iteratively until satisfying the convergence limit in each time step. Then the converged

efficiency factor (E_b). Each symbol represents the size and mass fraction of macroflocs, which were measured (the cross-hair symbol) and simulated (the filled symbol) at time = 180, 250, 490, 800, 1280, and 2180 s.

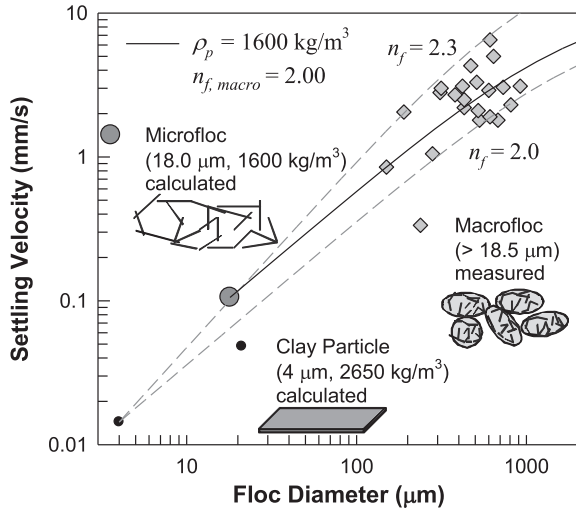


Fig. 6 – Plots of floc diameter versus settling velocity. The diamond symbols represent the measured diameter and settling velocity of a floc in settling column tests (van Leussen, 1994) and the lines represent the simulated data with the modified Stokes equation (Winterwerp, 2002). The schematic diagrams illustrate the floc packing strategies of microflocs and macroflocs with individual clay particles. Microflocs form by direct contact between clay minerals whereas macroflocs form by loose agglomeration between microflocs and organic matters (after van Leussen (1994)). ρ_p represents the density of microflocs and both n_f and $n_{f,macro}$ are the fractal dimension of macroflocs. The first and second numbers in the parentheses are the size and density of a floc, respectively.

values are used as the seeding values of the next time step (Other iteration methods should also be applicable.). All the simulations were done with the standard values of the kinetic and physicochemical factors and the initial conditions. The standard values of the kinetic and physicochemical factors were obtained from values found in previous studies (Jackson, 1995; Maggi, 2005; Winterwerp and van Kesteren, 2004), and the initial conditions were those measured in the settling column test (van Leussen, 1994) (Table 3).

To obtain optimum simulations of the column data, the collision efficiency factor (α) was used as the only adjustable fitting parameter in the model-data fitting analyses, while the other parameters were simply fixed at standard values found in the literature. This was done to reduce the complexity and uncertainty caused by many highly interactive parameters. The simulation quality was quantified by the sum of residual errors (SRE) between simulated and measured sediment concentrations (C_{sim} and C_{exp}) (Equation (10)) (Berthouex and Brown, 1994), with the minimum SRE defining the optimum simulation for the selected parameters.

$$SRE = \sum_{i=1}^n (\text{error}_i)^2 = \sum_{i=1}^n (C_{exp,i} - C_{sim,i})^2 \quad (10)$$

After the optimum α was selected, the sensitivity of the TCPBE to the kinetic and physicochemical parameters was evaluated by varying these parameters about their standard values.

3. Results and discussion

3.1. Comparison between the MCPBE, SCPBE, and TCPBE

Solutions of all PBEs produced U-shaped SRE curves with changes in the collision efficiency factor (α) (Fig. 2). Generally, as the fitting parameter (α) increases, the solid concentration profiles move downward, become the best fit curve by definition at the minimum SRE (Fig. 3), and further collapse downward, because the higher collision efficiency factor (α) increased the down-gradient flux of sediment by increasing floc size and settling velocity. The SRE of the TCPBE was slightly lower than the SRE of the MCPBE. However, by comparing the best fit solid concentration profiles the difference between the simulated concentration profiles of the TCPBE and MCPBE is shown to be relatively small (Fig. 3). Considering the sensitivity and uncertainty of contemporary flocculation models and experimental techniques (Fettweis, 2008), both the TCPBE and MCPBE are equally capable of simulating flocculation in the system tested using the data fitting procedure described. However, the SCPBE was obviously less capable by obtaining about 2–3 times higher SREs than the MCPBE and TCPBE. This represents the low-quality simulations of the SCPBE, which might be caused by the incapability of the SCPBE for simulating interactions between microflocs and macroflocs. The weaknesses of the SCPBE will be discussed further in the following paragraphs.

3.1.1. Solid concentration profiles

Fig. 3(a) shows the simulated (best-quality) and measured solid concentration profiles in the settling column test. Measured solid concentration profiles had low concentrations near the water surface, approached a concentration just above 1 g/L along the water depth and then a significant increase in solids concentration well above 1 g/L near the water bottom. Compared to the similar results of the MC and TC PBEs, the SCPBE curve was more above the data at early times and below the data at large times. This illustrates that the SCPBE was less able to fit the data compared to the MCPBE and TCPBE, possible due to the single size class limitation of the SCPBE.

Fig. 3(b) illustrates the potential superiority of the MCPBE in that bimodal floc size classes are actually calculated. However, the TCPBE could simulate two size peaks and the mass change of micro- and macro-flocs along the water depth as well as the MCPBE as it is currently formulated (Fig. 3). Considering that the TCPBE requires only three differential equations, its simplicity and capability are promising for large-scale simulation of a complicated marine and estuarine system. In contrast, the SCPBE with two differential equations could neither simulate well the early or late concentration data nor the bimodal mass changes because it simply tracks a single floc size class. One would expect this limitation to be even more prominent for a large-scale marine and estuarine system with a massive influx of fresh microflocs because the fate of fresh microflocs could not be tracked.

3.1.2. Floc size distribution details

Both the MC and TC PBEs could better simulate the size growth of flocs (D_f) in the initial growth phase ($t \leq 490$ s) and the final

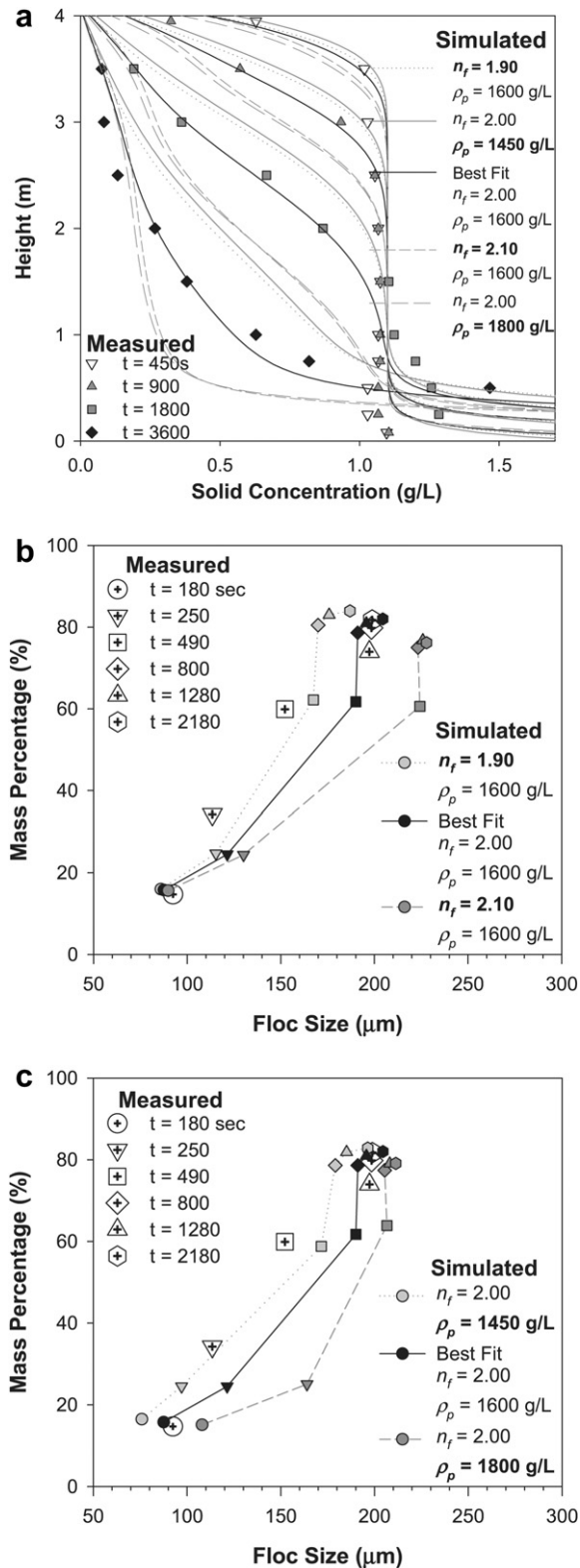


Fig. 7 – (a) Sensitivity of the solid concentration profiles of the TCPBE to the density of microflocs (ρ_p) and the fractal dimension of macroflocs (n_f). Symbols represent measured solid concentration profiles at time = 450, 900, 1800, and 3600 s. Lines represent simulated profiles with different density of microflocs (ρ_p) and fractal dimension of macroflocs (n_f). (b) sensitivity the size and mass fraction of

bimodal FSD in the steady state ($t \geq 800$ s) than the SCPBE (Fig. 4). (However, only the MCPBE generated a true bimodal size distribution.) For example, the TCPBE could track the size and mass fraction of microflocs and macroflocs while approximating the bimodal FSD in the initial growth phase and the steady state; the SCPBE approximates only a unimodal FSD. In Fig. 4, the “mean” floc sizes and mass fractions simulated with the TCPBE (dark sphere) could well follow the two peaks averaged from the measured FSD (triangle). Different to the MCPBE developing two peaks in a continuous manner, the TCPBE developed two sharp peaks of micro- and macroflocs. However, the SCPBE maintained a single sharp peak at a certain floc size in the initial growth phase and the steady state.

Furthermore, the SCPBE could not correctly estimate the settling flux of the bimodal FSD, which is the key index for estimating sediment deposition and transport in a marine or estuarine system. The settling flux ($\sum w_{s,i} \times C_i$ g/m²/sec) of the measured bimodal FSD was estimated to be 0.912 for 1 g/L solid concentration in the steady state ($t = 2180$ s). The simulated settling fluxes were estimated to be 0.938, 1.278, and 0.953 for the MCPBE, SCPBE, and TCPBE respectively. Noteworthy is that the simulated settling flux of the SCPBE had 40% error against the measured settling flux while the settling fluxes of the MCPBE and TCPBE had errors less than 5%. The SCPBE could not simulate 20% mass fraction of microflocs and consequently generated 40% error of the settling flux. This significant error propagation might be caused by the difference between the settling velocities of microflocs and macroflocs (≈ 0.106 and 1.14 mm/s, respectively) (Fettweis, 2008).

3.2. Model sensitivity to kinetic and physicochemical factors

After determining the “best fit to data” parameter values, the model sensitivity to kinetic and physicochemical parameter variations around the “best values” was investigated. Among numerous parameters shown in Table 3, (1) flocculation kinetic parameters – the aggregation and breakage efficiency factors (α and E_b), (2) floc structural parameters – the density of microflocs (ρ_p) and the fractal dimension of macroflocs (n_f), (3) fate of broken macroflocs – the mass fraction of microflocs generated by breakage of macroflocs (f), (4) initial conditions of seeded macroflocs for sweep flocculation – the size and mass fraction of seeded macroflocs ($D_{F,0}$ and $Frac_{F,0}$) were selected and model sensitivity tested. This was done by calculating the degree of deviation of simulations from the measured data – solid concentration profiles (e.g. Fig. 5(a)) and the mean size and mass fraction of macroflocs (e.g. Fig. 5(b) and (c)) which were calculated with the measured FSDs (Fig. 4).

macroflocs to the density of microflocs (ρ_p) and (c) sensitivity to the fractal dimension of macroflocs (n_f). Each symbol represents the size and mass fraction of macroflocs, which were measured (the cross-hair symbol) and simulated (the filled symbol) at time = 180, 250, 490, 800, 1280, and 2180 s.

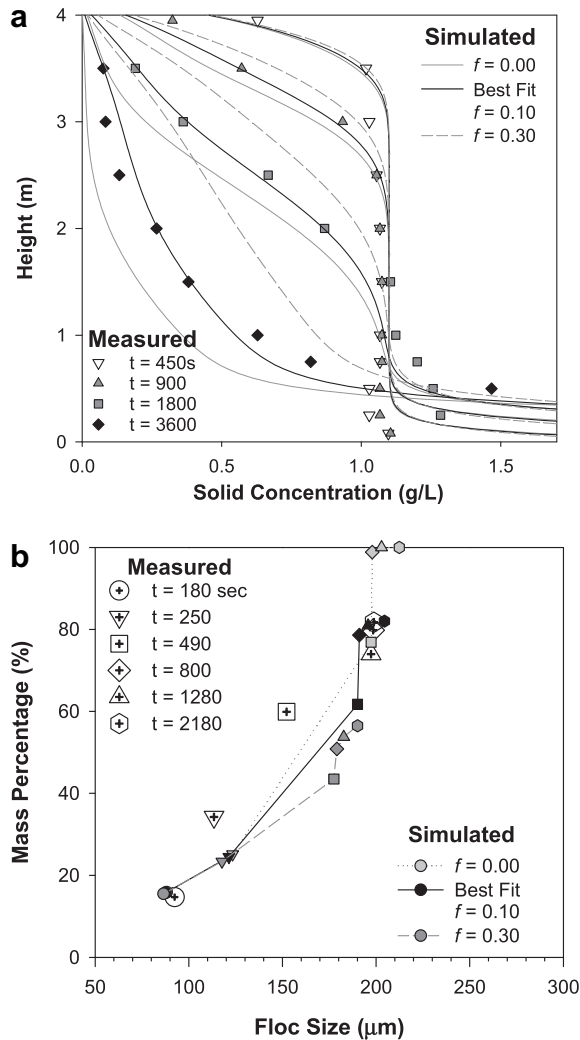


Fig. 8 – (a) Sensitivity of the solid concentration profiles of the TCPBE to the fraction of microflocs generated by breakage of macroflocs (f). Symbols represent measured solid concentration profiles at time = 450, 900, 1800, and 3600 s. Lines represent simulated profiles with different fraction of microflocs generated by breakage of macroflocs (f). (b) Sensitivity of the size and mass fraction of macroflocs to the fraction of microflocs generated by breakage of macroflocs (f). Each symbol represents the size and mass fraction of macroflocs, which were measured (the cross-hair symbol) and simulated (the filled symbol) at time = 180, 250, 490, 800, 1280, and 2180 s.

3.2.1. Flocculation kinetic parameters

The collision and breakage efficiency factors (α and E_b) cause in increase and decrease in floc size growth, respectively. For example, a higher collision efficiency factor ($\alpha = 0.15$) or a lower breakage efficiency factor ($E_b = 0.7 \times 10^{-4}$) both moved the solid concentration profiles downward (Fig. 5(a)). Either an increase in α or a decrease in E_b increased the size and mass fraction of macroflocs (Fig. 5(b) and (c)) which in turn increased the floc settling velocity. In contrast, a collision efficiency factor decrease ($\alpha = 0.05$) or a breakage efficiency factor increase ($E_b = 2.5 \times 10^{-4}$) moved the solid concentration

profiles upward (Fig. 5(b) and (c)). The interdependency between the collision and breakage efficiency factors in determining the overall flocculation kinetics agrees with the finding of Verney et al. (in press) and Maerz et al. (in press).

However, over time the respective changes of the collision and breakage efficiency factors (α and E_b) determined the size and mass fraction of macroflocs in a different manner. A change of the collision efficiency factor (α) differentiated the size and mass fraction of aggregating macroflocs in the initial growth phase ($t \leq 490$ s) (see the circle, triangle, and square symbols), but made a relatively small effect on the size and mass fraction of macroflocs at steady state ($t \geq 800$ s) (see the diamond, triangle, and hexagonal symbols in Fig. 5(b)). In contrast, the breakage efficiency factor (E_b) could differentiate the size and mass fraction of macroflocs in the steady state ($t \geq 800$ s). Thus, the collision efficiency factor (α) of the TCPBE determined the size and mass fraction of macroflocs mainly in the initial growth phase as a floc growth accelerator, while the breakage efficiency factor (E_b) was most effective near steady state as a floc-growth limiter (Equation (7) and Table 1).

3.2.2. Floc structural parameters

Unlike unimodal flocculation, bimodal flocculation involves microflocs and macroflocs. Thus, the TCPBE requires two distinct structures of less-porous and hard microflocs and highly-porous and floppy macroflocs (Fig. 6) (van Leussen, 1994; Winterwerp and van Kesteren, 2004). The structure of primary microflocs is characterized by their size and density (D_p and ρ_p), while the structure of aggregating macroflocs is determined by microflocs density (ρ_p) and macrofloc fractal dimension (n_f) (Table 2). Therefore, microfloc density (ρ_p) and macrofloc fractal dimension (n_f) were selected as the floc structural parameters for sensitivity analysis. Standard values for ρ_p and n_f ($\rho_p = 1600$ kg/m³ and $n_f = 2.0$, respectively) were selected from the literatures (Winterwerp and van Kesteren, 2004; Maggi, 2005). The standard values and the modified settling equations (Equations 8, 9) proved their validity by showing that simulated settling velocities were reasonably matched to measured velocities for different floc sizes (Fig. 6).

A higher microfloc density ($\rho_p = 1800$ kg/m³) or a higher macrofloc fractal dimension ($n_f = 2.10$) increased both the density of macroflocs (ρ_f) and the aggregation kinetics, and so moved the solid concentration profiles downward by increasing the size and settling velocity of macroflocs (Fig. 7 (a)). In contrast, a lower density for microflocs ($\rho_p = 1450$ kg/m³) or a lower fractal dimension of macroflocs ($n_f = 1.90$) moved the solid concentration profiles upward by decreasing the density of macroflocs and the aggregation kinetics. However, the respective changes of microfloc density (ρ_p) and macrofloc fractal dimension (n_f) occurred in different ways (Fig. 7(b) and (c)). For example, the effect of the fractal dimension of macroflocs (n_f) was more weighted on larger macroflocs while approaching steady state ($t \geq 490$ s) (Fig. 7 (b)). Considering that the fractal theory is based on an exponential relation between the sizes of microflocs and macroflocs (D_p and D_f Table 2 and Equation 11), the effect of the fractal dimension of macroflocs (n_f) should be exponential while increasing the macrofloc size. However, the density of microflocs (ρ_p) made rather a consistent effect on the size and mass fraction of macroflocs in the entire size range (Fig. 7(c))

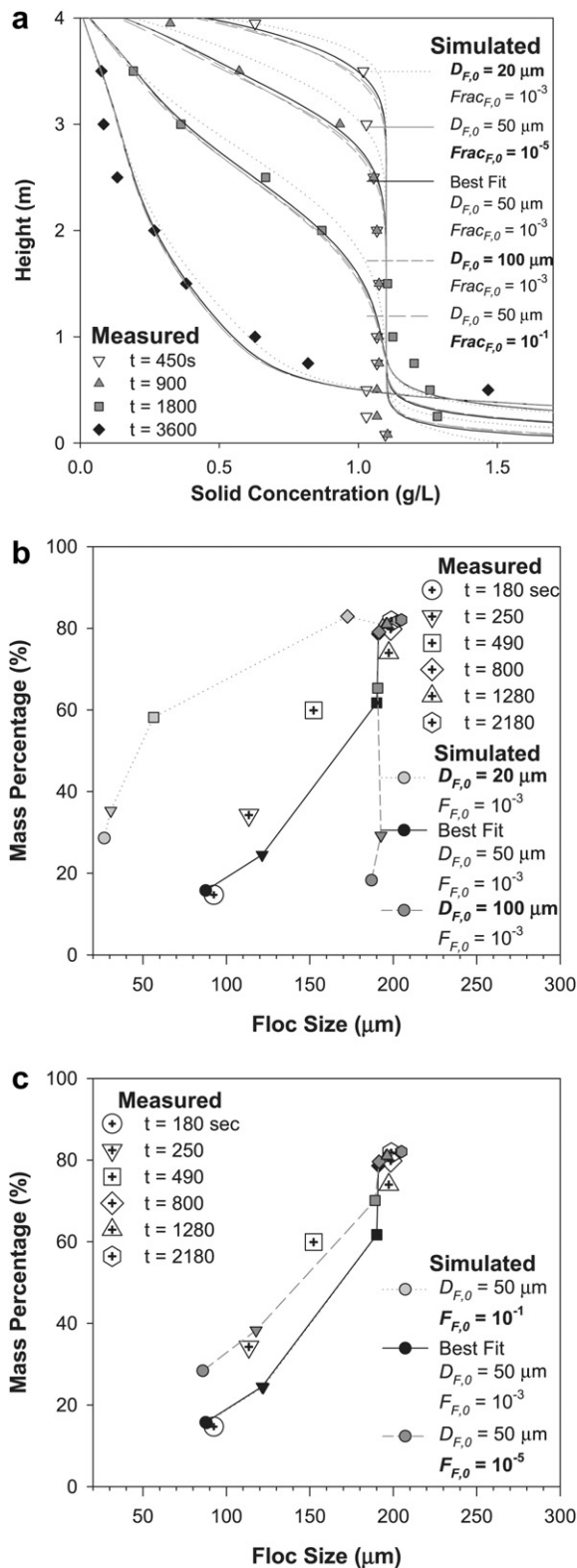


Fig. 9 – (a) Sensitivity of the solid concentration profiles of the TCPBE to the size and mass fraction of seeded macroflocs ($D_{F,0}$ and $Frac_{F,0}$). Symbols represent measured solid concentration profiles at time = 450, 900, 1800, and 3600 s. Lines represent simulated profiles with different size and mass fraction of seeded macroflocs ($D_{F,0}$ and $Frac_{F,0}$). (b) Sensitivity of the size and mass fraction of

because of the linear relation between the densities of microflocs and macroflocs (ρ_p and ρ_F) (Equation 11). The sensitivity to the floc structural parameters was not as significant as the sensitivity in simulation of Maerz et al. (in press), in which a ± 0.2 variation of fractal dimension doubled an average floc size. The smaller sensitivity to the floc structural parameters might occur in the steady flow condition of the 1-D settling column than in the unsteady flow condition of the shear-varying reactor (Maerz et al., in press).

$$\rho_F = \rho_w + (\rho_p + \rho_w) \left[\frac{D_p}{D_F} \right]^{3-n_f} \quad (11)$$

3.2.3. Distribution of fragmented flocs

Sediments in the settling column still had a 20% mass fraction of microflocs while approaching the steady state ($t \geq 800$ s Fig. 4). This residual mass fraction of microflocs was hypothesized to occur by fragmentation of macroflocs to microflocs. The fragmentation process was formulated with the additional parameter of the fraction of microflocs generated by breakage of macroflocs (f), and incorporated into the TCPBE as shown in Equation (7) and Table 1. The fragmentation process of the TCPBE has a similar theoretical background and mathematical formula to the one of the size class-based flocculation model (Verney et al., in press). The TCPBE with the fragmentation process ($f = 0.1$) could better simulate the long tail of the solid concentration profile at the last measuring time ($t = 3600$ s Fig. 8(a)) and the residual mass fraction of microflocs ($= 1 - \{\text{the mass fraction of macroflocs}\}$) in the steady state ($t \geq 800$ s Figs. 4 and 8(b)). However, without a fraction of microflocs generated by breakage of macroflocs ($f = 0$), the long solid tail at $t = 3600$ s disappeared near the water surface, and the mass fractions of microflocs and macroflocs became zero and one, respectively, in the steady state, because all microflocs agglomerated to macroflocs. In contrast, a higher fraction of microflocs generated by breakage of macroflocs ($f = 0.3$) reduced the down-gradient flux of solid concentration profiles by decreasing the mass fraction of macroflocs but increasing the mass fraction of microflocs (Fig. 8). In fact, the fraction of microflocs generated by breakage of macroflocs (f) could determine both the solid concentration profiles and the size and mass fraction of macroflocs. Considering that the breakage and fragmentation processes are highly dependent on the fluid shear rate (G Table 2), the fraction of microflocs generated by breakage of macroflocs (f) should be more important for predicting the fate of sediments (e.g. solid concentration profiles and FSDs) under the varying shear rate in a marine and estuarine system (e.g. Verney et al., in press) than in the well-controlled settling column test studied herein.

3.2.4. Initial conditions of seeded macroflocs

Sweep flocculation describes flocculation in which seeded macroflocs enmesh surrounding particles or microflocs in

macroflocs to the size of seeded macroflocs ($D_{F,0}$) and (c) sensitivity to the mass fraction of seeded macroflocs ($Frac_{F,0}$). Each symbol represents the size and mass fraction of macroflocs, which were measured (the cross-hair symbol) and simulated (the filled symbol) at time = 180, 250, 490, 800, 1280, and 2180 s.

a fluid shear field and enhance the floc growth and the bimodality of an FSD. Sweep flocculation is commonly applied in water treatment, and enhances flocculation by metal-hydroxide macroflocs collecting small impure particles or microflocs (Gregory, 2006). In a marine or estuarine system, sweep flocculation can be similarly defined as flocculation of sticky organic-bound macroflocs collecting nearby microflocs. Considering the sudden appearance of a substantial amount of large macroflocs without a sequential floc growth in the initial growth phase (Fig. 4), sweep flocculation might also occur in the settling column test. A very small amount of macroflocs surviving the preliminary breaking and homogenizing step was hypothesized to function as seeded macroflocs for sweep flocculation. Therefore, different sizes ($D_{F,0} = 20, 50$ and $100 \mu\text{m}$) and mass fractions ($\text{Frac}_{F,0} = 0.001, 0.1$ and 10%) of seeded macroflocs were tested as initial conditions in simulations for investigating sweep flocculation.

The solid concentration profiles remained almost consistent, irrespective of the change of the initial conditions of seeded macroflocs ($D_{F,0}$ and $\text{Frac}_{F,0}$) (Fig. 9(a)). However, the size and mass fraction of macroflocs were changed significantly by the initial size of seeded macroflocs ($D_{F,0}$), especially in the initial growth phase ($t \leq 490$ s) but not in the steady state ($t \geq 800$ s). For example, macroflocs slowly grew up to the final size of macroflocs of the steady state with the smaller seeded macroflocs ($D_{F,0} = 20 \mu\text{m}$), but they rapidly grew with the larger seeded macroflocs ($D_{F,0} = 100 \mu\text{m}$) (Fig. 9(b)). However, these different initial macrofloc-growth patterns had a minor effect on the solid concentration profiles. Sedimentation continued even after the macrofloc size became constant at steady state ($t \geq 800$ s), and thus was more dependent on the size and settling velocity of macroflocs. Therefore, as long as the size and mass fraction of macroflocs remained relatively constant a steady state, like the case shown in Fig. 9(b) and (c), the solid concentration profiles were close each other due to similar rates of sedimentation. However, a very small amount of seeded macroflocs (e.g. $\text{Frac}_{F,0} = 0.001\%$ and $D_{F,0} = 50 \mu\text{m}$) is necessary to correctly simulate the sweep flocculation and bimodal FSDs of aggregating macroflocs in the TCPBE.

4. Conclusion and recommendation

The two-class PBE was shown to be the simplest model that is capable of approximating bimodal flocculation of marine and estuarine sediments. In contrast to the SCPBE, the TCPBE can simulate bimodal interactions between micro- and macroflocs and thus estimate the collector capability of a marine or estuarine system for fresh microflocs supplied by an upstream river. Compared to the MCPBE, the TCPBE incorporates simplicity and computational efficiency at the expense of producing non-detailed floc size distributions. In an average floc size sense, however, it can be used to simulate large-scale sediment transport in marine and estuarine environments in a practical manner. Against the recent class-based and distribution-based models (Verney et al., in press and Maerz et al., in press), the TCPBE has the simplicity to require less computational cost and the capability to simulate bimodal flocculation, respectively, and is easy for marine engineers or scientists to adopt it without numerical and mathematical

background. For example, the TCPBE can be easily solved by commercial or in-house differential equation solvers and thus free users from effort for programming. Furthermore, the TCPBE allows one to include the effect of additional biological and physicochemical processes on flocculation, such as interactions between micro-organisms and inorganic flocs or adsorption of natural organic matter with ease and flexibility (Maggi, 2009). Therefore, the TCPBE may be used as a practical model for investigation of the highly complicated fate of marine and estuarine sediments by incorporating other coupled equations of micro-organisms, organic matter, and so on. While the MCPBE may be ultimately superior in simulating these coupled processes and producing realistic floc size distributions, the experimental and computational work required to realize such superiority is significant.

The two-class PBE as well as the other PBEs still require fine adjustment for their aggregation and breakage kinetics. Well-controlled flocculation experiments may be required to find realistic kinetic and physicochemical parameters. Only in the last decade, have various investigators began using PBEs for simulating flocculation in a marine and estuarine systems. Thus, experimental data, which can be used for estimating kinetic and physicochemical parameters of the PBEs, are still limited. A serious bias may sometimes occur by extrapolating the PBEs out of the boundary of experimental data. In fact, intensive investigation on the aggregation and breakage kinetics will be required for improved application of the PBEs in marine and estuarine systems.

Acknowledgment

The authors would like to acknowledge the Flemish Science Foundation (FWO Vlaanderen) for funding the FWO project no. G.0263.08. Wim van Leussen kindly allowed the authors to use the experimental data of his PhD dissertation.

REFERENCES

- Aro, C., Rodrigue, G., Rotman, D., 1999. A high performance chemical kinetics algorithm for 3-D atmospheric models. The International Journal of High Performance Computing Applications 13 (1), 3–15.
- Berthouex, P., Brown, L., 1994. Statistics for Environmental Engineers. Lewis Publishers, Boca Raton, FL.
- Burd, A., Jackson, G., 2002. Modeling steady-state particle size spectra. Environmental Science and Technology 36, 323–327.
- Chen, M., Wartel, S., Temmerman, S., 2005. Seasonal variation of floc characteristics on tidal flats, the Scheldt estuary. Hydrobiologia 540, 181–195.
- Curran, K., Hill, P., Milligan, T., 2002. Fine-grained suspended sediment dynamics in the Eel River flood plume. Continental Shelf Research 22, 2537–2550.
- Curran, K., Hill, P., Milligan, T., Cowan, E., Syvitski, J., Konings, S., 2004. Fine-grained sediment flocculation below the Hubbard Glacier meltwater plume, Disenchantment Bay, Alaska. Marine Geology 203, 83–94.
- Curran, K., Hill, P., Milligan, T., Mikkelsen, O., Law, B., Durrieu de Madron, X., et al., 2007. Settling velocity, effective density, and mass composition of suspended sediment in a coastal bottom

- boundary layer, Gulf of Lions, France. *Continental Shelf Research* 27, 1408–1421.
- Ding, A., Hounslow, M., Biggs, C., 2006. Population balance modelling of activated sludge flocculation: investigating the size dependence of aggregation, breakage and collision efficiency. *Chemical Engineering Science* 61, 63–74.
- Droppo, I., Leppard, G., Liss, S., Milligan, T., 2005. *Flocculation in Natural and Engineered Environmental Systems*. CRC Press, Boca Raton, FL, USA.
- Li, Y., Wolanski, E., Xie, Q., 1993. Coagulation and settling of suspended sediment in the Jiaojiang river estuary, China. *Journal of Coastal Research* 9 (2), 390–402.
- Li, B., Eisma, D., Xie, Q., Kalf, J., Li, Y., Xia, X., 1999. Concentration, clay mineral composition and Coulter counter size distribution of suspended sediment in the turbidity maximum of the Jiaojiang river estuary, Zhejiang, China. *Journal of Sea Research* 42, 105–116.
- Fettweis, M., 2008. Uncertainty of excess density and settling velocity of mud floccs derived from in situ measurements. *Estuarine, Coastal and Shelf Science* 78 (2), 426–436.
- Fox, R., 2003. *Computational Models for Turbulent Reacting Flows*. Cambridge University Press, Cambridge UK.
- Gregory, J., 2006. *Particles in Water: Properties and Processes*. CRC Press, Boca Raton, FL, USA.
- Hill, P., Milligan, T., Rockwell Geyer, W., 2000. Controls on effective settling velocity of suspended sediment in the Eel River flood plume. *Continental Shelf Research* 20, 2095–2111.
- Hounslow, M., Ryall, R., Marshall, V., 1988. A discretized population balance for nucleation, growth, and aggregation. *AIChE Journal* 34 (1), 1821–1832.
- Jackson, G., 1995. Comparing observed changes in particle size spectra with those predicted using coagulation theory. *Deep-Sea Research II* 42 (1), 159–184.
- Jackson, G., Logan, B., Alldredge, A., Dam, A., 1995. Combining particle size spectra from a mesocosm experiment measured using photographic and aperture impedance (Coulter and Elzone) technique. *Deep-Sea Research* 42 (1), 139–157.
- Jeong, J., Choi, M., 2003. A simple bimodal model for the evolution of non-spherical particles undergoing nucleation, coagulation and coalescence. *Journal of Aerosol Science* 34, 965–976.
- Jeong, J., Choi, M., 2004. A bimodal moment model for the simulation of particle growth. *Journal of Aerosol Science* 35, 1071–1090.
- Jeong, J., Choi, M., 2005. A bimodal particle dynamics model considering coagulation, coalescence and surface growth, and its application to the growth of titania aggregates. *Journal of Colloid and Interface Science* 281, 351–359.
- Krishnappan, B., Marsalek, J., 2002. Modelling of flocculation and transport of cohesive sediment from an on-stream stormwater detention pond. *Water Research* 36, 3849–3859.
- Kusters, K., 1991. *The Influence of Turbulence on Aggregation of Small Particles in Agitated Vessels*. Eindhoven University of Technology, the Netherlands.
- van Leussen, W., 1994. *Estuarine Macroflots: Their Role in Fine-grained Sediment Transport*. Universiteit van Utrecht, the Netherlands.
- Maerz, J., Verney, R., Wirtz, K., Feudel, U. Modeling flocculation processes: intercomparison of a size class-based model and a distribution-based model. *Continental Shelf Research*, in press, corrected proof. doi:10.1016/j.csr.2010.05.011.
- Maggi, F., 2005. *Flocculation Dynamics of Cohesive Sediment*. Technische Universiteit Delft, the Netherlands.
- Maggi, F., 2009. Biological flocculation of suspended particles in nutrient-rich aqueous ecosystems. *Journal of Hydrology* 376, 116–125.
- Manning, A., Bass, S., 2006. Variability in cohesive sediment settling fluxes: observations under different estuarine tidal conditions. *Marine Geology* 235, 177–192.
- Manning, A., Bass, S., Dyer, K., 2006. Floc properties in the turbidity maximum of a mesotidal estuary during neap and spring tidal conditions. *Marine Geology* 235, 193–211.
- Manning, A., Friend, P., Prowse, N., Amos, C., 2007a. Estuarine mud flocculation properties determined using an annular mini-flume and the LabSFLOC system. *Continental Shelf Research* 27, 1080–1095.
- Manning, A., Martens, C., de Mulder, T., Vanlede, J., Winterwerp, J., Ganderton, P., et al., 2007b. Mud floc observations in the turbidity maximum zone of the Scheldt estuary during neap tides. *Journal of Coastal Research SI* 50, 832–836.
- Megaridis, C., Dobbins, R., 1990. A bimodal integral solution of the dynamic equation for an aerosol undergoing simultaneous particle inception and coagulation. *Aerosol Science and Technology* 12, 240–255.
- Mietta, F., Chassagne, C., Winterwerp, J., 2009. Shear-induced flocculation of a suspension of kaolinite as function of pH and salt concentration. *Journal of Colloid and Interface Science* 336, 134–141.
- Mietta, F., Chassagne, C., Manning, A., Winterwerp, J. Influence of shear rate, organic matter content, pH and salinity on mud flocculation. *Ocean Dynamics, PECS 2008 Special Issue*, in press.
- Mikkelsen, O., Pejrup, M., 2001. The use of a LISST-100 laser particle sizer for in-situ estimates of floc size, density and settling velocity. *Geo-Marine Letters* 20, 187–195.
- Mikkelsen, O., Hill, P., Milligan, T., 2006. Single-grain, microfloc and macrofloc volume variations observed with a LISST-100 and a digital floc camera. *Journal of Sea Research* 55, 87–102.
- Mueller, M., Blanquart, G., Pitsch, H., 2009a. A joint volume-surface model of soot aggregation with the method of moments. *Proceedings of the Combustion Institute* 32, 785–792.
- Mueller, M., Blanquart, G., Pitsch, H., 2009b. Hybrid Method of Moments for modeling soot formation and growth. *Combustion and Flame* 156, 1143–1155.
- Orange, D., Garcia-Garcia, A., Lorenson, T., Nittrouer, C., Milligan, T., Miserocchi, S., et al., 2005. Shallow gas and flood deposition on the Po Delta. *Marine Geology* 222-223, 159–177.
- Periane, R., 2005. Modelling the transport of suspended particulate matter by the Rhone River plume (France). Implications for pollutant dispersion. *Environmental Pollution* 133, 351–364.
- Peterson, E., 1965. *Chemical Reaction Analysis*. Prentice Hall, Englewood Cliffs, NJ, US.
- Prat, O., Ducoste, J., 2006. Modeling spatial distribution of floc size in turbulent processes using the quadrature method of moment and computational fluid dynamics. *Chemical Engineering Science* 59, 685–697.
- Richardson, J., Zaki, W., 1954. Sedimentation and fluidisation, Part I. *Transactions of the American Institute of Chemical Engineers* 2, 35–53.
- van Rijn, L., 1984. Sediment transport. Part II: suspended load transport. *Journal of Hydraulic Engineering* 110 (11), 1613–1641.
- van Rijn, L., 2007. Unified View of sediment transport by Currents and Waves. II: suspended transport. *Journal of Hydraulic Engineering* 133 (6), 668–689.
- Schiller, L., 1932. *Fallversuche mit kugeln und scheiben in Handbuch der experimental-Physik*. Akademische Verlagsgesellschaft, Leipzig.
- Son, M., Hsu, T., 2008. Flocculation model of cohesive sediment using variable fractal dimension. *Environmental Fluid Mechanics* 8, 55–71.
- Son, M., Hsu, T., 2009. The effect of variable yield strength and variable fractal dimension on flocculation of cohesive sediment. *Water Research* 43, 3582–3592.

- Spicer, P., Pratsinis, S., 1996. Coagulation-fragmentation: universal steady state particle size distribution. *AIChE Journal* 42, 1612.
- Toorman, E., 1999. Sedimentation and self-weight consolidation: constitutive equations and numerical modelling. *Geotechnique* 49 (6), 709–726.
- Verney, R., Lafite, R., Brun-Cottan, J., 2009. Flocculation potential of estuarine particles: the importance of environmental factors and of the spatial and seasonal variability of suspended particulate matter. *Estuaries and Coasts* 32, 678–693.
- Verney, R., Lafite, R., Claude Brun-Cottan, J., Le Hir, P. Behaviour of a floc population during a tidal cycle: laboratory experiments and numerical modelling. *Continental Shelf Research*, in press, corrected proof. doi:10.1016/j.csr.2010.02.005.
- Winterwerp, J., 2002. On the flocculation and settling velocity of estuarine mud. *Continental Shelf Research* 22, 1339–1360.
- Winterwerp, J., van Kesteren, W., 2004. Introduction to the Physics of Cohesive Sediment in the Marine Environment. Elsevier B.V, Amsterdam, The Netherlands.
- Yuan, Y., Wei, H., Zhao, L., Cao, Y., 2009. Implications of intermittent turbulent bursts for sediment resuspension in a coastal bottom boundary layer: a field study in the western Yellow Sea, China. *Marine Geology* 263, 87–96.